Self-Assembly and Cathodoluminescence of Microbelts from Cu-Doped Boron Nitride Nanotubes

Zhi-Gang Chen,[†,‡] Jin Zou,[§] Qingfeng Liu,[†] Chenghua Sun,[‡] Gang Liu,[†] Xiangdong Yao,[‡] Feng Li,[†] Bo Wu,[†] Xiao-Li Yuan,[¶] Takashi Sekiguchi,[¶] Hui-Ming Cheng,[†,*] and Gao Qing Lu[‡,*]

[†]Shenyang National Laboratory for Materials Science, Institute of Metal Research, Chinese Academy of Sciences, Shenyang 110016, China, [‡]ARC Centre of Excellence for Functional Nanomaterials, School of Engineering and AIBN, The University of Queensland, Brisbane QLD 4072, Australia, [§]School of Engineering and Centre for Microscopy and Microanalysis, The University of Queensland, Brisbane QLD 4072, Australia, and [¶]Advanced Electronic Materials Center, National Institute for Materials Science, 1-1 Namiki, Tsukuba, Ibaraki 305-0044, Japan

ABSTRACT We report the self-assembly of microbelts from Cu-doped boron nitride nanotubes by chemical vapor deposition using Cu as a catalyst. The BN nanotubes with Cu-encapsulated flat tips have uniform outer diameters of ~240 nm, inner diameters of ~210 nm, and lengths of ~10 μm, and Cu is found to uniformly dope into the nanotubes. Most importantly, the nanotubes are self-assembled to form microbelts with 10 μm in width and tens of micrometers in length. Strong and tunable light emissions from the ultraviolet to visible light range are observed in such Cu-doped microbelts, showing their high potential for applications in lasing, light-emitting diode, and medical diagnosis devices.

KEYWORDS: boron nitride nanotubes · Cu · microbelt · self-assembly · cathodoluminescence · dope

Since individual nanostructures can function as both device elements and interconnects, semiconductor nanotubes (NTs) have been widely recognized as building blocks in assembling active devices and systems.[1–4] This concept has been demonstrated in nanoelectronics with the assembly of a variety of devices, such as field-effect transistors,[5] integrated logic gates,[2] individual light-emitting diodes, and laser diodes.[6] Actually, many existing and emerging electronic/optoelectronic devices can benefit from the integration of semiconductor nanomaterials into a single system in either two-dimensional (2D) or 3D layouts.[7] Bottom-up assembly and epitaxial growth of nanoscale building blocks into increasingly complex structures represent the two most widely used methods for achieving these types of integrated systems. Self-assembly is emerging as an elegant, bottom-up method for fabricating semiconductor nanomaterials. This approach becomes particularly powerful when the ease and control offered by the self-assembly of semiconductor nanomaterials is coupled with their superior electronic, magnetic, or photonic properties.[8]

Boron nitride NTs (BNNTs), a wide gap semiconductor nanostructure with a band gap independent of their morphologies and/or geometries,[9] have increasingly attracted wide research interest. Due to their excellent optical[10] and mechanical properties,[11] high thermal conductivity,[12] good oxidation resistivity,[13] and chemical inertness,[14] BNNTs show great potential for applications as unique electromechanical and optoelectronic components for laser, light-emitting diode, and medical diagnosis. Various BN nanostructures, such as NTs,[15] nanobamboos,[16] nanohorns,[17] nanowires,[18] and yard-glass BNNTs[19] have been reported. A wide range of catalysts,[20] such as Fe, Ni, Co, Mg,[21] and metal oxides,[22] have been used to synthesize BN nanostructures by different methods including arc-discharge,[15] laser heating/ablation,[23] ball milling−annealing,[24] carbon nanotube substitution,[25] soft chemical method,[26] and chemical vapor deposition (CVD).[27] However, rational assembly of BNNTs is still a challenge with low quality and nonuniformed structures. It is of great significance to search for more efficient catalysts to *in situ* self-assemble of BNNTs for integrated systems and practical applications. Cu can be used to synthesize inorganic nanowires[28,29] and to catalyze carbon NTs (CNTs)[30] and carbon nanofibers,[31] though theoretical calculation suggests that Cu shows poor catalytic efficiency for CNT growth.[32] Recently, one convincing result was reported that Cu is a good catalyst for the growth of single-walled CNTs (SWNTs), especially for the preparation of long hori-

*Address correspondence to cheng@imr.ac.cn, maxlu@uq.edu.au.

Received for review April 6, 2008 and accepted July 09, 2008.

Published online July 29, 2008.
10.1021/nn800211z CCC: $40.75

zontal arrays of SWNTs.[33] Moreover, new physical/chemical phenomena that the Cu/Au catalyst not only catalyzes the growth of semiconductor inorganic nanowires (such as GaAs and Si) but also migrates on the surface of semiconductor nanowires were observed.[29,34] However, there is no report of using Cu to directly catalyze and dope BN nanostructures.

The chemistry of NTs is intriguing because their internal hollow cavity can serve as a nanoreactor or channel for catalysis, drug delivery, separation, storage, encapsulation, and transport of various molecules.[3] There is a potential to use larger, uniform inner diameter NTs as reactors or channels, which motivates us to design and fabricate architectures with large inner cavities based on the crystallographic characteristics and intrinsic properties of the materials.

In this study, we show self-assembly of high quality microbelts composed of Cu-doped BNNTs with a large inner diameter and flat tips *via* a Cu-catalyzed CVD method. Our experimental results prove that Cu can act as a catalyst for the fabrication of BNNTs and self-assembling BNNTs to form microbelts. Cu doping and Cu filling[35] in the BNNTs will greatly benefit their electronic and optoelectronic properties. We demonstrate that a tunable visible light emission can be excited from Cu-doped BN microbelts, similar to that from Eu-doped BNNTs.[36] The unique light emission is due to the Cu^{2+} ions doping in the BNNTs, so that BN microbelts can serve as a host and contribute directly to the light emission.

RESULTS AND DISCUSSION

The general morphology of the synthesized BN architectures was examined by scanning electron microscopy (SEM) as shown in Figure 1a−c. Figure 1a displays a typical belt-like morphology, which is approximate 10 μm in width and tens of micrometers in length. High-resolution (HR) SEM images (Figure 1b,c) show that the microbelts consist of a large number of self-assembled nanotubes, which grew along an angle of ~60° with respect to the edge of the microbelt. A catalyst is commonly found to be located at the top of each nanotube. Figure 1d−f shows several typical HRSEM images of an individual microbelt. Figure 1d clearly shows that the microbelt consists of numerous well-aligned NTs. One single NT peeled out from the microbelt shows a sword-shape with a catalyst tip, a straight body, and a wallow-tail with catalytic tip as well (Figure 1e), and interestingly, all NTs have a flat tip (Figure 1f). Moreover, their diameters tend to be similar. By analyzing several hundreds of NTs, their diameter distribution was determined and is shown in Figure 1g. More than 90% of NTs have their outer diameters in the range between 230 and 250 nm, with a Gaussian mean diameter of ~240 nm. This suggests that the synthesized NTs have a good diameter uniformity which is critical to the chemical applications of NTs.[3] The XRD pattern of the synthesized product is shown in Figure 1h, from which two crystalline phases can be clearly identified: hexagonal BN (JCPDS: 34-0431: $a = 0.2504$ nm and $b = 0.6656$ nm) and cubic Cu (JCPDS: 04-0836; $a = 0.3615$ nm). No characteristic peaks arising from other impurities, such as CuO, were detected in the XRD pattern. On the basis of the XRD results, we can confirm that (1) the NTs must be BN and (2) the catalysts (shown as the bright clusters in Figure 1f) must be pure Cu.

Detailed microstructure characterizations of the microbelts are illustrated in TEM images (Figure 2). They are self-assembled nanotubes oriented in the angle of ~ 60° with respect to the edge of the microbelts (Figure 2a), forming fan-like arrays with knob-like bottoms welded by multiple junction tails (Figure 2b), which may be one reason for good alignment. A much clearer image (Figure 2c) shows the tubes with a uniform diameter of ~240 nm and a nanoparticle at their tip with a particle size of ~100 nm. One interesting point worthy of emphasizing is that the tube has a flat tip. We also occasionally observed some single BNNTs peeled out from the arrays, having a sword-sheath shape with a catalyst-encapsulated tip, a straight body, and a wallow-tail also with a catalyst-encapsulated tip as shown in Figure 2d. Such characteristics will help us to understand the growth mechanism which will be discussed later. The energy-dispersive X-ray spectroscopy (EDS) of the catalyst and NT is shown in Figure 2e,f. In Figure 2e, a typical EDS taken from the catalyst-encapsulated flat tips at the nickel grid shows the characteristic ionization edges of B, N, and Cu. This confirms that the catalyst nanoparticles are Cu, which matches well with the XRD result. No O and C were found in the EDS profile. Furthermore, the EDS analysis on the body of the tube as shown in Figure 2f gives the ratio of B/N close to 1, and a little Cu about 0.4% compared to B and N content is detected.

To further determine their chemical compositions, energy filtered (EF) TEM was used to map elements of B, N, and Cu. Images were formed with the energy loss windows centered at the B K edge of 188 eV, the N K edge of 401 eV, and the Cu K edge of 931 eV. Figure 3a is an image using electrons with zero energy loss showing the morphology of a section of a microbelt. Figure 3b,c shows B and N maps of the section and clearly the presence of B and N. Figure 3d is a Cu map in which the catalyst at the tip is clearly shown. More importantly, Cu signals in the tube section were observed, indicating that Cu is doped into the tubes. This is consistent with the EDS analysis, as shown in Figure 2f. Figure 3e is the overlapped image of B, N, and Cu maps.

High-resolution electron energy loss spectroscopy (EELS) was used to study several tens of nanotubes to further characterize their composition. Figure 4a is a typical EELS profile of an individual nanotube in which two distinct edges at 188 and 401 eV are revealed, cor-

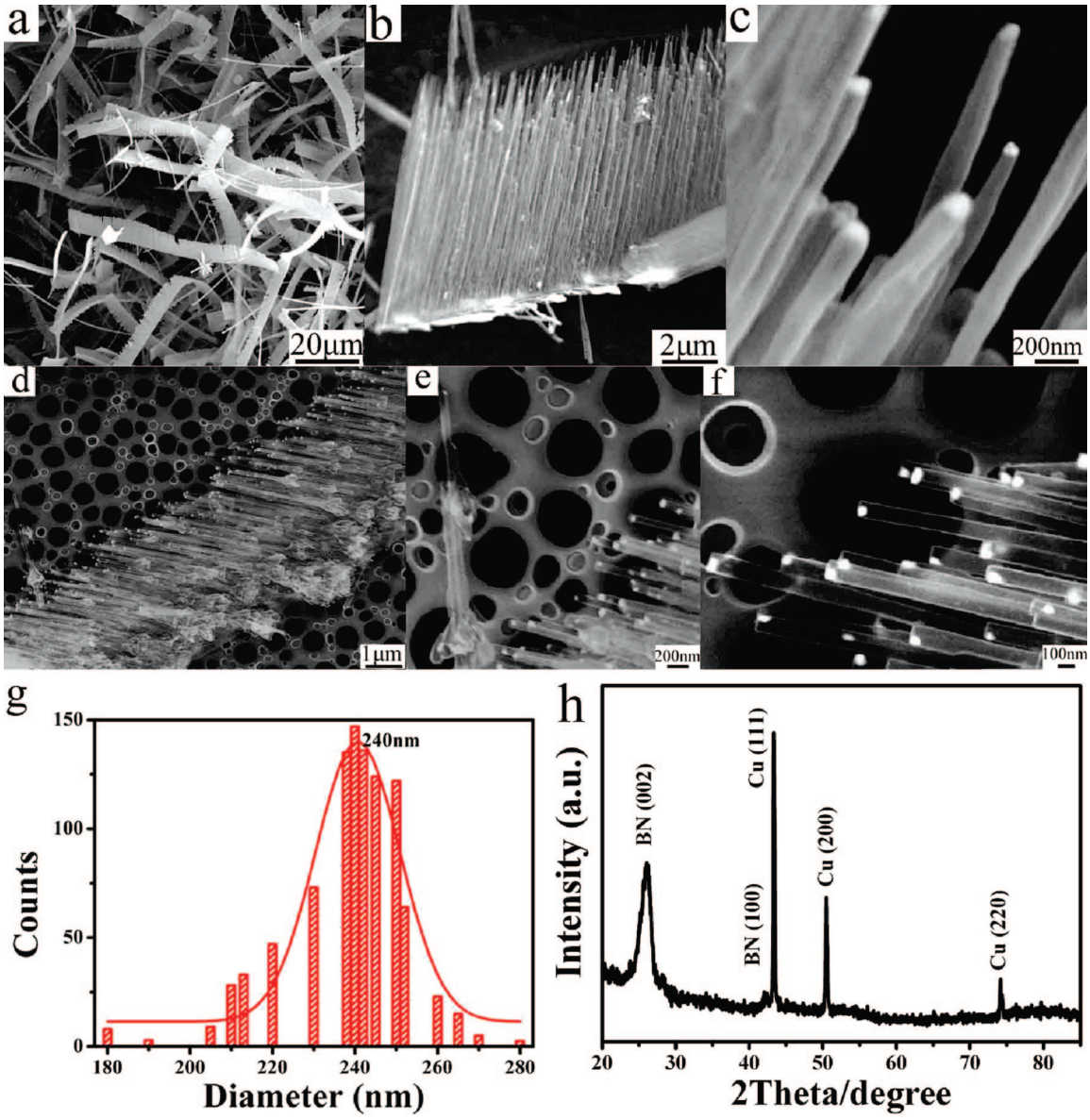

Figure 1. (a−c) SEM images of the product showing typical belt-like morphology with a catalyst tip. (d−f) SEM images of the product showing that the microbelts consist of arrays of numerous NTs with a flat tip. (g) Outer diameter distribution and (h) XRD spectrum of the product.

responding to the B−K and N−K edges, respectively. The sharp π* peaks on the left side of both K edges confirm that the nanotubes are composed of sp^2-bonded B and N atoms. Quantification of EELS spectra gives a B/N atomic ratio of 1.0 ± 0.20. No O signal is observed from the inset in Figure 4a, indicating that BNNTs are oxygen-free. Figure 4b represents the Cu $L_{2,3}$ edges of the signals measured from the tip and body of Cu-doped BNNTs, as well as the signals from standard metallic Cu and CuO.[37] The two major features of these edges are the white lines L_3 and L_2, due to the spin orbit splitting of the 2p core hole.[37] By comparing the measured shapes and intensity of Cu $L_{2,3}$ edges of Cu-doped BNNTs with those standards, it can be clearly seen that the EELS profile of the catalyst is close to that of metallic Cu while the EELS profile of the nanotube is similar to that of CuO, indicating that the majority of Cu in the tubes is Cu^{2+} (*i.e.*, doped state).

To further understand the Cu state in doped BN microbelts, X-ray photoelectron spectroscopy (XPS) analysis was used to detect the fresh surface and Ar^+ sputtered surface of the product in order to distinguish doped Cu and metallic Cu in the BNNTs, in which the B 1s, N 1s, and Cu 2p core-level regions are examined, as shown in Figure 5. It shows that the sample surface consists of nitrogen and boron with binding energies of N 1s and B 1s at 398.7 and 191.5 eV, respectively, indicating that the product has B−N bonding. The quantification of the peak intensities reveals that the atomic ratio of B−N is 1:1, which agrees well with the chemical stoichiometric relation between B and N and EELS analysis. The XPS Cu 2p core-level spectra detected

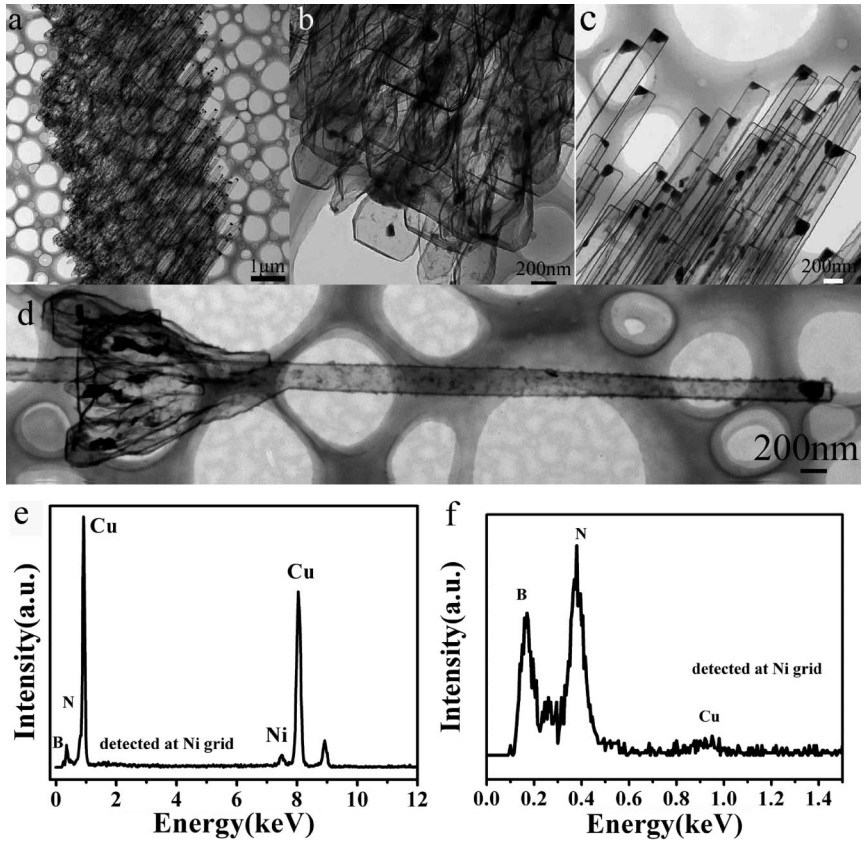

Figure 2. TEM images of a microbelt. (a) Low magnification image, (b) roots of the BNNT array, (c) flat tips with a catalyst, (d) a single tube peeling from the microbelts, (e) EDS profiles of the catalysts at the nickel grid, and (f) EDS profile of the body of BNNTs.

from the fresh surface of the BN microbelts and surface after Ar^+ sputtering for 600 s are shown in Figure 5c. Relatively weak Cu $2p_{3/2}$ and Cu $2p_{1/2}$ peaks at 933.0 and 955.9 eV can be observed from the fresh surface, while strong peaks at ~932.7 and 954.9 eV are detected after Ar^+ sputtering. From the database of the XPS, Cu can have various bonding states, such as Cu^0, Cu^{1+}, and Cu^{2+}. It has been reported that, for Cu-doped Manganite spinels,[38] the peak at 930.7 eV could be assigned to Cu^+, the peak at 933.0 eV to Cu^{2+},[38] and Cu^0 should be in the value range between 932.7 and 932.5 eV. Therefore, the XPS spectra shown in Figure 5c can be deconvoluted and assigned. Cu $2p_{3/2}$ and Cu $2p_{1/2}$ peaks at 933.0 and 955.9 eV can be assigned to Cu^{2+}, indicating that Cu ions were doped into the BNNTs. The quantification of the peak intensities of B, N, and Cu suggests a Cu doping level of approximately <0.4 at % when it is considered that some signals are from the encapsulated Cu nanoparticles. Cu $2p_{3/2}$ and Cu $2p_{1/2}$ peaks at 932.7 and 954.9 eV can be assigned to Cu^0, indicating that a certain quantity of encapsulated Cu nanoparticles must be naked after Ar^+ sputtered for 600 s. Comparisons between the peak intensity and position of these two spectra further substantiate that the Cu doping state may be Cu^{2+}.

To investigate the possible doping sites of Cu atoms, theoretical calculations were employed in the framework of density functional theory (DFT). First, it is found that the interaction of B and Cu is stronger than N and Cu, suggesting that Cu atoms prefer to distribute around B. Five structural models are proposed, as marked by (A−E) in Figure 6a, where B, N, and Cu are indicated as pink, blue, and black spheres. On the basis of the optimized geometry, the bonding energies (BE) were calculated by $BE = E_{Cu\text{-}BN} - (E_{Cu} + E_{BN})$, as presented in Figure 6b. Among the five models, only model C is not stable. It is also found that chemical adsorption on the surface and in the inner cavity of BNNTs shows higher stability than the adsorption between two neighboring layers, indicating that these adsorptions may serve as the main doping form.

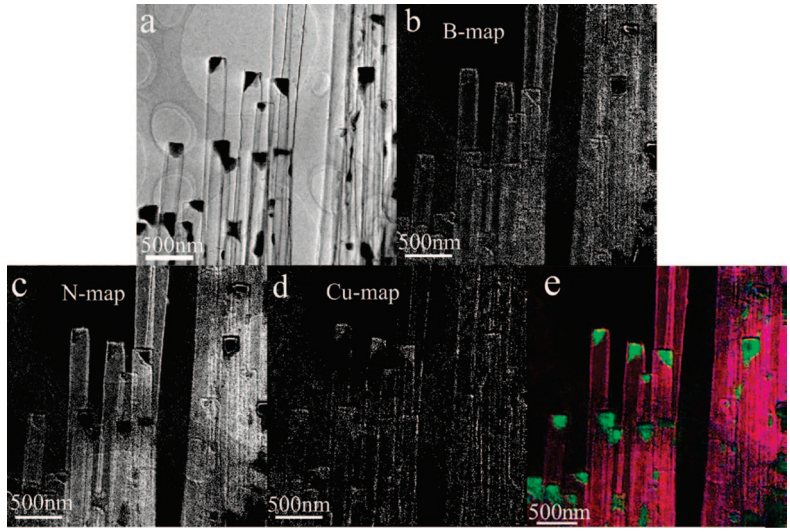

Figure 3. (a) Zero-loss image of a section of one microbelt. (b−d) Elemental maps (B, N, and Cu) of the section of the microbelt. (e) Image of overlapped maps shows chemical composition of the microbelt.

To explore the atomic structure of individual tubes, we performed a detailed HRTEM study. Figure 7a illustrates a typical BNNT with a diameter of ~240 nm. The tube has a clean and remarkably thin wall with a flat tip. The electron diffraction (ED)

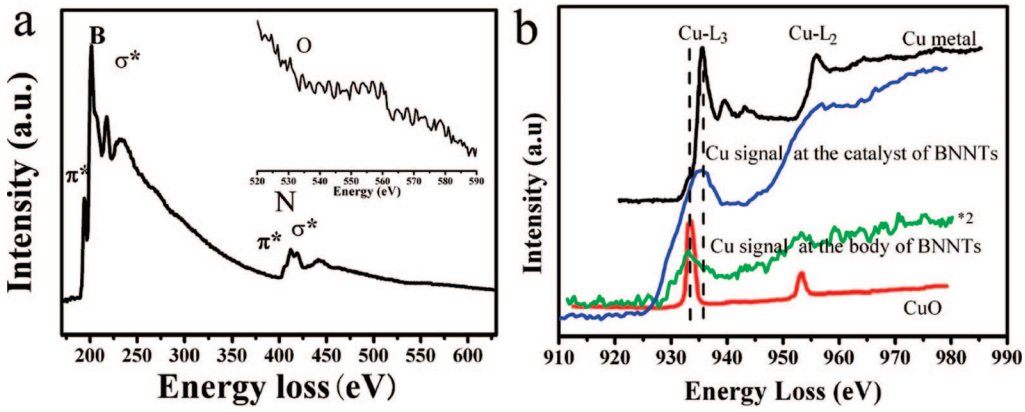

Figure 4. EELS spectra from a responsive tube. (a) EELS spectra of B, N, O, and inset showing the high-resolution EELS spectrum of O. (b) Comparison between the Cu $L_{2,3}$ of reference metal copper, copper oxide, and the sample studied at the tip and the body of BNNTs.

pattern (Figure 7b) taken from the corresponding tubular wall exhibits a regular reflection, indicating that the tube has a high crystallinity. In the ED pattern, a pair of bright arcs peculiar to the (002) and (004) reflections are visible along the direction perpendicular to the conical axis. Furthermore, the pattern also displays a pair of $(10\bar{1}0)$ and $(11\bar{2}0)$ arcs along the tubular axis. These results suggest that the (002) planes near the external edge of the tube are preferentially oriented parallel to the incidental electron beam. The ED pattern suggests that the tube wall consists of cylindrically stacked BN graphite-like (002) planes. Figure 7c depicts a tube wall segment with a wall thickness of ~15 nm. The wall is built up of nearly 40 BN graphite-like layers. It clearly shows the (002) lattice fringes with an interplanar spacing of 0.34 nm within the tube wall and the $(10\bar{1}0)$ lattice fringes of 0.22 nm. Moreover, the inner diameters of about 1000 isolated nanotubes were measured with average value of ~210 nm at an accuracy of ±1 nm based on HRTEM images, as shown in Figure 7d. Figure 7e shows the HRTEM image of the catalyst. The Cu particle grows along the [200] direction, and the direction of the epitaxial crystallization on the BNNTs is [0002]. One important structural characteristic is that the angle between the $[200]_{Cu}$ and $[0002]_{BN}$ directions is ~120°. Such a crystallographic characteristic is a key factor in controlling all the tubes assembled to an array along ~60°. The inset image in Figure 7e illustrates the fast Fourier transform (FET) diffraction, which is indexed as a [011] zone axis of a face-centered cubic structure with (111) plane spacing of ~0.21 nm.

The self-assembly mechanism of microbelts from BNNTs can be determined through examining samples grown at different stages, as illustrated in Figure 8. Fig-

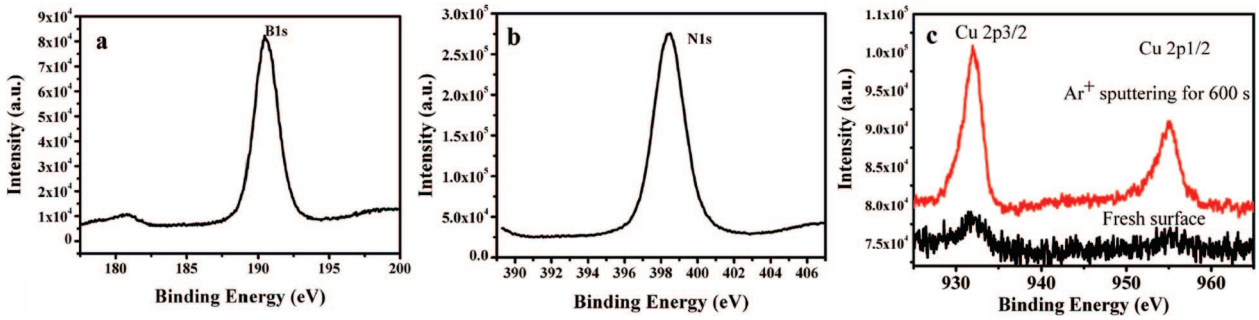

Figure 5. XPS spectra of BNNT microbelts in B 1s (a), N 1s (b), and Cu 2p (c) core-level regions from fresh surface and Ar^+ sputtered surface.

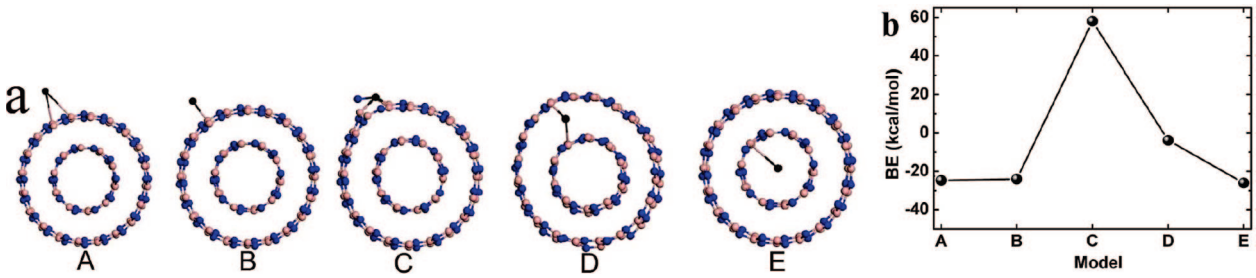

Figure 6. (a) Five structural chemical adsorption B−Cu models: A (two bond) and B (one bond) on the surface; C, in the framework; D, between BN layers; E, in the inner cavity. (b) Bonding energies (BE) calculated by BE = $E_{Cu\text{-}BN} - (E_{Cu} + E_{BN})$.

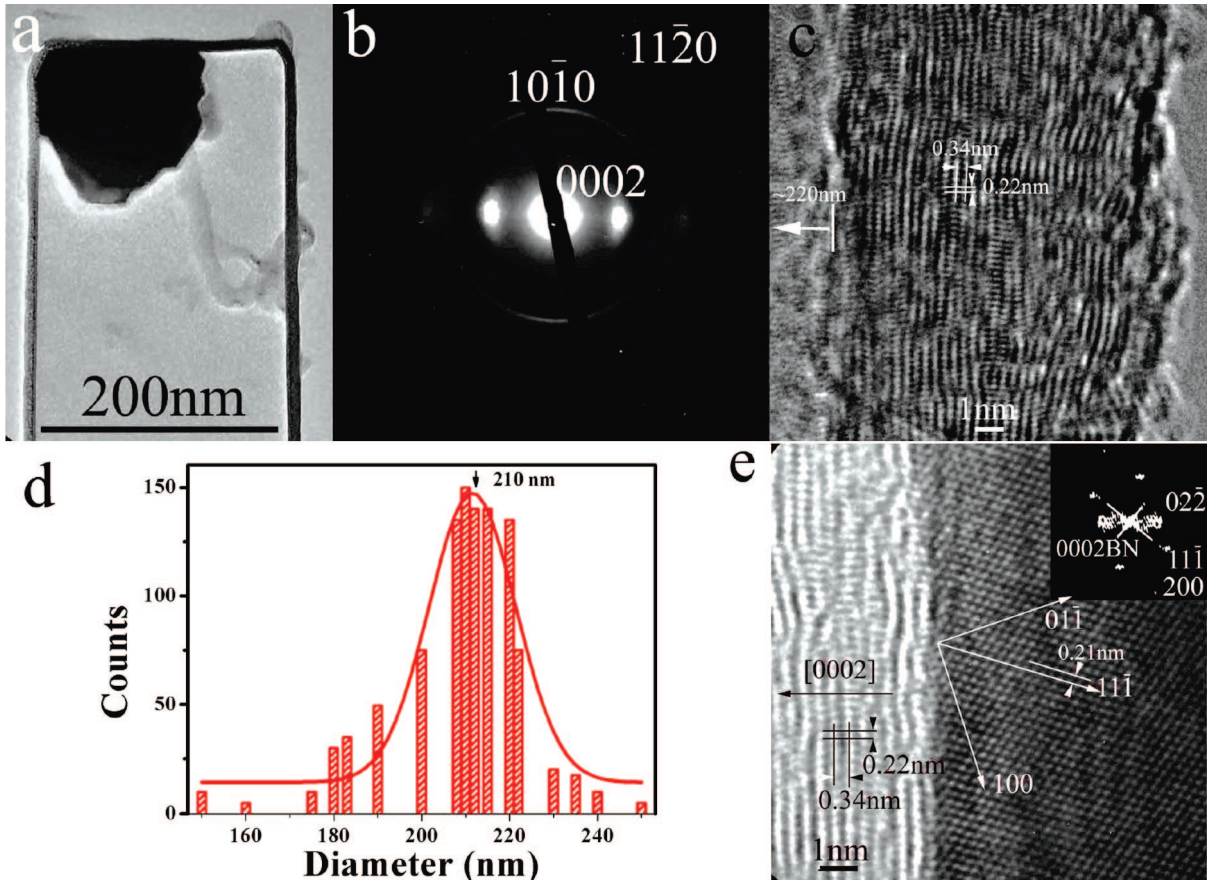

Figure 7. (a) TEM image showing a BNNT with a closed flat end. (b) SEAD pattern of the NT body. (c) HRTEM image taken from the BN wall (wall thickness ~15 nm). (d) Inner diameter distribution of the nanotubes. (e) HRTEM image of a Cu catalyst, and inset is its corresponding fast Fourier transform (FFT) diffraction.

ure 8a is a BN fiber filled with many Cu catalysts formed in the initial stage. Such a fiber has swallow-like knobs, which is similar to the roots of BNNTs (Figure 1d and Figure 2b) with large diameter catalyst filled. The diameters of about 300 isolated catalysts were measured with an accuracy of ±2 nm based on TEM images, as shown in Figure 8b, and it is large with a Gaussian mean diameter of ~450 nm. The final product shown in Figure 8c is a microbelt with BNNT arrays and sward-sheath shape knobs, which leads us to believe that the tube arrays are grown from the fiber. The diameters of about several hundreds isolated catalysts in the tubes were measured, with an accuracy of ±1 nm based on TEM images. As shown in Figure 8d, the diameter is uniform and has a Gaussian mean diameter of ~100 nm. Compared with the catalysts in the initial fiber, it is evident that a large quantity of Cu particles splitted into smaller ones and remained at the tube tips, and at the same time, a certain amount of Cu was doped into the tubes (which was confirmed by above EELS, elemental mapping, and XPS analysis). Therefore, it is reasonable to conclude that Cu played a critical role in the formation of such novel structures. First, B−O precursors vaporize and react with NH_3 to form B/N clusters at 1240 °C. At the same time, Cu slowly vaporizes (melting point, 1083 °C). Vaporized Cu and B/N clusters move downstream at the temperature of 1000 °C. At this temperature, Cu may form nanosized liquid droplets (nanosized Cu should have a lower melting point than that of the bulk Cu), which provides energetically favorable sites for B/N cluster nucleation based on a vapor−liquid−solid (VLS) growth mechanism.[39] The boron and nitrogen atoms diffuse into the Cu liquid droplets to form a Cu−B−N solution from which BNNTs grow out according to the VLS growth mechanism. A little Cu in the ion state may dope into the BN graphite-like layer during growth. The formation of microbelts is due to interaction between the sward-sheath shaped roots of NTs. The diameter of BNNTs and the size of catalysts in the tips of BNNTs are uniform. We consider that the diameter of BNNTs must be controlled by the crystallographic characteristics (facet, particle size) and growth crystallographic direction of the Cu catalyst, supported by our structural analysis with SEM and TEM observations. It is known that B has a higher solubility in Cu solid or liquid solution than that of N, but the solubility of B/N in Cu is quite low based on the Cu/B and Cu/N binary phase diagrams, which indicate that B/N can precipitate out more easily from Cu−B−N quasi-solution. Since conventional catalysts, such as Fe, Co, and Ni, have a high solubility of B or N. As a result, the Cu-catalyzed processes should be distinctly different

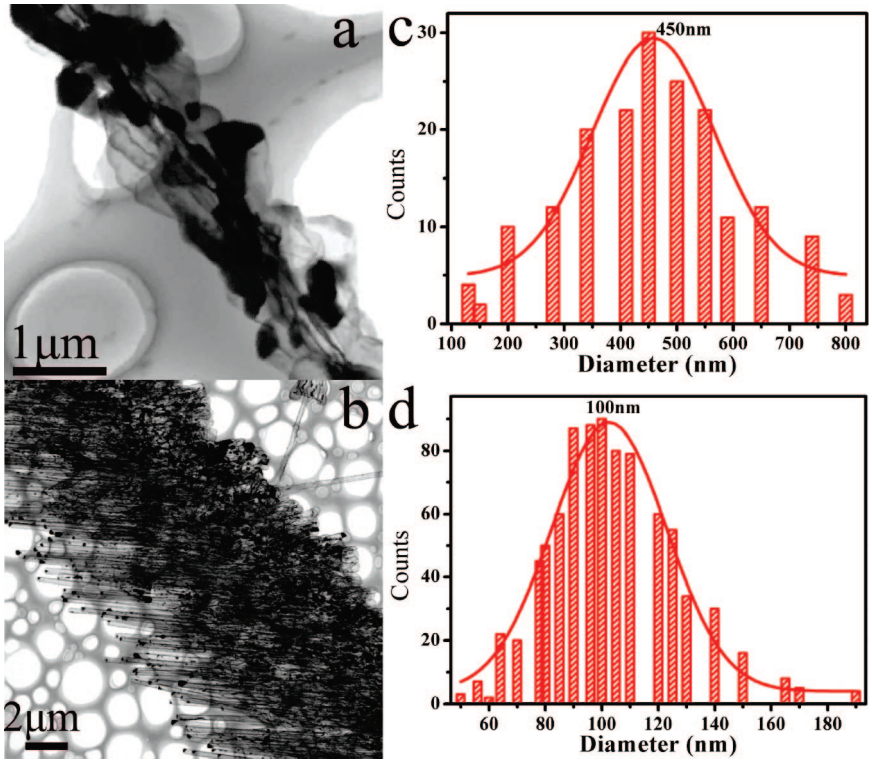

Figure 8. Initial and final stage of the microbelt growth. (a) Initial stage forming a fiber with Cu catalysts. (b) Diameter distribution of Cu catalysts in this initial stage. (c) Final stage array of short BNNTs growing from a fiber. (d) Diameter distribution of Cu catalysts inside BNNTs.

from those catalyzed by conventional catalysts. In addition, Cu has low catalytic activity of B/N clusters, and then the supply of B/N clusters in the process is slow and relatively low. Matching the supply of the B/N clusters and the formation of NTs will produce remarkably thin walls of BNNTs. Another remarkable aspect of the present structures is that all the NTs have flat tips, which is similar to other observations,[40,41] and was explained as a combination of three declinations in the hexagonal BN network.[40]

One of the key applications of BN and its architectures is in optoelectronic devices. Therefore, we analyzed the cathodoluminescent (CL) properties of the product microbelts. Figure 9a,b shows SEM images of the BNNT microbelts and its corresponding room temperature SEM-CL image taken at a wavelength of 330 nm, showing a uniform contrast which indicates uniform CL properties across the whole microbelts assembled from Cu-doped BNNTs. The luminescence intensity is homogeneous along the tube, and the catalyst tips cannot be seen, suggesting no contribution to the CL emission from the Cu tip particles. Figure 9c−e shows the CL spectra taken from undoped and doped nanotubes with two different Cu contents at room temperature. The insets are corresponding XPS analysis of Cu, which gives the Cu content of 0.4 and 0.1 atom % Cu for the samples in Figure 9d,e. Figure 9c shows a typical CL spectrum of BN nanostructures, which is similar to those reported by Sekiguchi *et al.*,[42] Zhang *et al.*,[43] and Zhi *et al.*[44] The spectrum is basically composed of a relatively broad emission peak that can be deconvoluted into two peaks (major centered on 330 and 380 nm). The peak (330 nm, corresponding to 3.75 eV) is a typical CL emission from hexagonal BN structure or multiwalled cylindrical BNNTs,[10,44] excited by a high energy electron. Such ultraviolet light emission was very stable after the sample was irradiated for 10 min. The peak (380 nm, corresponding to 3.26 eV) is most likely associated with the large diameter and relatively thin wall of BNNTs, as the emission at the same energy range was

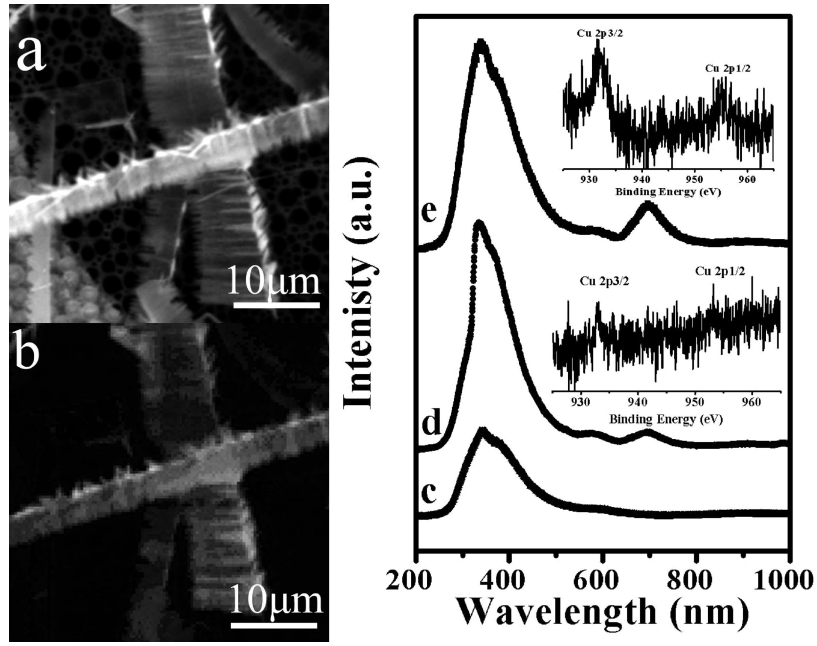

Figure 9. (a) SEM image of the Cu-doped BNNT assembled microbelts on a nickel grid. (b) Their CL-SEM image. CL spectra of the BNNT microbelts: (c) undoped BNNTs; (d) 0.1 atom % Cu; (e) 0.4 atom % Cu.

observed from BNNTs,[10,17] suggesting that they are attributed to deep-level emissions associated with defect-related centers (B or N vacancy-type defect-trapped states).[10,43] For Cu-doped NTs (Figure 9d,e), the spectra have a new strong band emission centered at around 695 nm (corresponding to 1.78 eV) in addition to the two CL emission peaks. Clearly, the strong visible peak is attributed to the doped Cu, and its intensity increases with increasing Cu content. This new visible light emission should be associated with the radiative transition emission of Cu^{2+} in the Cu-doped BN architectures. The strong interactions between large Cu atoms and BN basal atomic planes maintain the Cu^{2+} ion state, and therefore, the BNNT host (not carriers) significantly influences the surrounding environment of Cu^{2+} ions and subsequently changes the band splitting of the crystal field and configurations.[45,46] Visible emissions at 490 nm from Eu-doped bamboo BNNTs[36] and around 550 nm from Si-doped bamboo BNNTs[47] have already been reported. Compared to these results, the peak at 695 nm in our work is near-red emission. The band structures of BNNTs have been investigated both theoretically and experimentally,[48–50] and the reported electronic structures can be tuned between 1 and 5.8 eV by the direct band gap and radiative transitons.[50] Han *et al.*[50] reported that the CL spectra between 3.0 and 4.2 eV are due to radiative transitions which could be generated by a replacement of some N atoms with O. Figure 9 demonstrates that light emission from the Cu-doped BN architectures can be tuned from the near-UV to visible light range by Cu doping. Moreover, the intensity of the visible light emission peak can be adjusted by changing the excitation voltage, and the light emission can be changed by varying the Cu doping content.

CONCLUSIONS

To conclude, novel microbelts self-assembled from Cu-doped multiwalled BNNTs were synthesized by the Cu-catalyzed CVD method. The nanotubes have uniform outer diameters of ~240 nm, inner diameter of ~210 nm, and a length of ~10 μm. Cu is found to be filled into the tips and uniformly doped into the nanotubes. Most significantly, the nanotubes are self-assembled to form a microbelt. Strong and red-light emission at 695 nm due to the doping of Cu^{2+} ions in BNNTs is observed and is expected to be very useful in lighting sources and possibly also in other electromechanical and optoelectronic devices such as laser, light-emitting diode, and medical diagnosis devices.

METHODS

Micobelts self-assembled from boron nitride nanotubes were fabricated by chemical vapor deposition. High-purity Ar (at a rate of 150 sccm) and NH_3 (at a rate of 175 sccm) were used as the carrier gas and reaction gas. The raw materials—a ball-milled mixture of B−O precursors (mass ratio: B:B_2O_3 = 1:7 and nano-Cu powders (mean diameter about 50 nm)—were loaded into an Al_2O_3 crucible at the center of a quartz tube (diameter of 32 cm, length of 100 cm), which was located in the horizontal tube furnace. The temperature of the furnace was increased at a rate of 35 °C min^{-1} to 1240 °C and was maintained at that temperature for 120 min for synthesis of hierarchical BNNTs. After 2 h, a white film-like product was collected at the down place of stream, where temperature should be 1000 °C when the furnace was at the 1240 °C.

The synthesized products were comprehensively characterized using X-ray diffraction (XRD, RINT2200, Cu Kα), scanning electron microscopy (SEM, JEOL 6400F, and JEOL 890), and transmission electron microscopy (TEM, FEI Tecnai F30 equipped with electron energy loss spectroscopy (EELS) and energy-dispersive X-ray spectroscopy (EDS)).

Spatially resolved CL measurements and *in situ* CL imaging of BN microbelts were carried out (TFE-SEM, Hitachi S4200). The samples were first deposited on a standard nickel TEM grid and thoroughly characterized using TEM and were then used for CL characterization. CL spectra of BN microbelts were collected using a high-resolution CL system operating at an accelerating voltage of 5 kV and a current of 1.2 nA.

Computational Methods. To investigate the doping sites of Cu atoms at the electronic level, the geometric and total energies of Cu-doped BNNTs with five models were calculated in the framework of density functional theory (DFT), within the generalized gradient approximation (GGA)[51] and the exchange-correlation functional of Perdew−Burke−Ernzerhof (PBE).[52] Core electrons were described based on effective core potentials, and double-numeric quality basis sets[53–55] were employed in the expansion of the molecular orbitals. All the calculations were carried out by using DMol3 code.

Acknowledgment. This work was supported by the Key Research Program of MOST, China (2006CB932703), and Australian Research Council. The authors also thank to H. Guo, D. M. Tang, C. Liu, and X. L. Ma for kind assistance and discussion. C.S. thanks S. C. Smith and CCMS for the usage of DMol3 package.

REFERENCES AND NOTES

1. Goldberger, J.; Fan, R.; Yang, P. D. Inorganic Nanotubes: A Novel Platform for Nanofluidics. *Acc. Chem. Res.* **2006**, *39*, 239–248.
2. Bachtold, A.; Hadley, P.; Nakanishi, T.; Dekker, C. Logic Circuits with Carbon Nanotube Transistors. *Science* **2001**, *294*, 1317–1320.
3. Baughman, R. H.; Zakhidov, A. A.; de Heer, W. A. Carbon Nanotubes—The Route Toward Applications. *Science* **2002**, *297*, 787–792.
4. Kongkanand, A.; Kamat, P. V. Electron Storage in Single Wall Carbon Nanotubes. Fermi Level Equilibration in Semiconductor−SWCNT Suspensions. *Acs Nano* **2007**, *1*, 13–21.
5. Lin, Y. M.; Appenzeller, J.; Chen, Z. H.; Chen, Z. G.; Cheng, H. M.; Avouris, P. High-Performance Dual-Gate Carbon Nanotube FETs with 40-nm Gate Length. *IEEE Electron Device Lett.* **2005**, *26*, 823–825.
6. Zhang, M.; Fang, S. L.; Zakhidov, A. A.; Lee, S. B.; Aliev, A. E.; Williams, C. D.; Atkinson, K. R.; Baughman, R. H. Strong, Transparent, Multifunctional, Carbon Nanotube Sheets. *Science* **2005**, *309*, 1215–1219.
7. Ahn, J.-H.; Kim, H.-S.; Lee, K. J.; Jeon, S.; Kang, S. J.; Sun, Y.; Nuzzo, R. G.; Rogers, J. A. Heterogeneous Three-Dimensional Electronics by Use of Printed Semiconductor Nanomaterials. *Science* **2006**, *314*, 1754–1757.
8. Thurn-Albrecht, T.; Schotter, J.; Kastle, C. A.; Emley, N.; Shibauchi, T.; Krusin-Elbaum, L.; Guarini, K.; Black, C. T.; Tuominen, M. T.; Russell, T. P. Ultrahigh-Density Nanowire Arrays Grown in Self-Assembled Diblock Copolymer Templates. *Science* **2000**, *290*, 2126–2129.

9. Blase, X.; Rubio, A.; Louie, S. G.; Cohen, M. L. Stability and Band-Gap Constancy of Boron-Nitride Nanotubes. *Europhys. Lett.* **1994**, *28*, 335–340.
10. Lauret, J. S.; Arenal, R.; Ducastelle, F.; Loiseau, A.; Cau, M.; Attal-Tretout, B.; Rosencher, E.; Goux-Capes, L. Optical Transitions in Single-Wall Boron Nitride Nanotubes. *Phys. Rev. Lett.* **2005**, *94*, 037405–037407.
11. Vaccarini, L.; Goze, C.; Henrard, L.; Hernandez, E.; Bernier, P.; Rubio, A. Mechanical and Electronic Properties of Carbon and Boron-Nitride Nanotubes. *Carbon* **2000**, *38*, 1681–1690.
12. Chang, C. W.; Fennimore, A. M.; Afanasiev, A.; Okawa, D.; Ikuno, T.; Garcia, H.; Li, D. Y.; Majumdar, A.; Zettl, A. Isotope Effect on the Thermal Conductivity of Boron Nitride Nanotubes. *Phys. Rev. Lett.* **2006**, *97*, 085901-1–085901-4.
13. Chen, Y.; Zou, J.; Campbell, S. J.; Le Caer, G. Boron Nitride Nanotubes: Pronounced Resistance to Oxidation. *Appl. Phys. Lett.* **2004**, *84*, 2430–2432.
14. Golberg, D.; Bando, Y.; Kurashima, K.; Sato, T. Synthesis and Characterization of Ropes Made of BN Multiwalled Nanotubes. *Scripta Mater.* **2001**, *44*, 1561–1565.
15. Chopra, N. G.; Luyken, R. J.; Cherrey, K.; Crespi, V. H.; Cohen, M. L.; Louie, S. G.; Zettl, A. Boron-Nitride Nanotubes. *Science* **1995**, *269*, 966–967.
16. Ma, R. Z.; Bando, Y.; Sato, T. Controlled Synthesis of BN Nanotubes, Nanobamboos, and Nanocables. *Adv. Mater.* **2002**, *14*, 366–368.
17. Zhi, C. Y.; Bando, Y.; Tang, C. C.; Golberg, D.; Xie, R. G.; Sekiguchi, T. Large-Scale Fabrication of Boron Nitride Nanohorn. *Appl. Phys. Lett.* **2005**, *87*, 63107–63109.
18. Huo, K. F.; Hu, Z.; Chen, F.; Fu, J. J.; Chen, Y.; Liu, B. H.; Ding, J.; Dong, Z. L.; White, T. Synthesis of Boron Nitride Nanowires. *Appl. Phys. Lett.* **2002**, *80*, 3611–3613.
19. Chen, Z. G.; Zou, J.; Li, F.; Liu, G.; Tang, D. M.; Li, D.; Liu, C.; Ma, X. L.; Cheng, H. M.; Lu, G. Q. Growth of Magnetic Yard-Glass Shaped Boron Nitride Nanotubes with Periodic Iron Nanoparticles. *Adv. Funct. Mater.* **2007**, *17*, 3371–3376.
20. Golberg, D.; Bando, Y.; Tang, C. C.; Zhi, C. Y. Boron Nitride Nanotubes. *Adv. Mater.* **2007**, *19*, 2413–2432.
21. Tang, C.; Bando, Y.; Sato, T.; Kurashima, K. A Novel Precursor for Synthesis of Pure Boron Nitride Nanotubes. *Chem. Commun.* **2002**, 1290–1291.
22. Golberg, D.; Bando, Y.; Bourgeois, L.; Kurashima, K.; Sato, T. Insights into the Structure of BN Nanotubes. *Appl. Phys. Lett.* **2000**, *77*, 1979–1981.
23. Golberg, D.; Bando, Y.; Eremets, M.; Takemura, K.; Kurashima, K.; Yusa, H. Nanotubes in Boron Nitride Laser Heated at High Pressure. *Appl. Phys. Lett.* **1996**, *69*, 2045–2047.
24. Chen, Y.; Chadderton, L. T.; Fitzgerald, J.; Williams, J. S. A Solid-State Process for Formation of Boron Nitride Nanotubes. *Appl. Phys. Lett.* **1999**, *74*, 2960–2962.
25. Han, W. Q.; Mickelson, W.; Cumings, J.; Zettl, A. Transformation of $B_xC_yN_z$ Nanotubes to Pure BN Nanotubes. *Appl. Phys. Lett.* **2002**, *81*, 1110–1112.
26. Xu, L. Q.; Peng, Y. Y.; Meng, Z. Y.; Yu, W. C.; Zhang, S. Y.; Liu, X. M.; Qian, Y. T. A Co-Pyrolysis Method to Boron Nitride Nanotubes at Relative Low Temperature. *Chem. Mater.* **2003**, *15*, 2675–2680.
27. Lourie, O. R.; Jones, C. R.; Bartlett, B. M.; Gibbons, P. C.; Ruoff, R. S.; Buhro, W. E. CVD Growth of Boron Nitride Nanotubes. *Chem. Mater.* **2000**, *12*, 1808–1810.
28. Nguyen, P.; Ng, H. T.; Meyyappan, M. Catalyst Metal Selection for Synthesis of Inorganic Nanowires. *Adv. Mater.* **2005**, *17*, 1773–1777.
29. Arbiol, J.; Kalache, B.; Cabarrocas, P. R. I.; Morante, J. R.; Morral, A. F. I. Influence of Cu as a Catalyst on the Properties of Silicon Nanowires Synthesized by the Vapour−Solid−Solid Mechanism. *Nanotechnology* **2007**, *18*, 305606.
30. Tao, X. Y.; Zhang, X. B.; Cheng, J. P.; Wang, Y. W.; Liu, F.; Luo, Z. Q. Synthesis of Novel Multi-Branched Carbon Nanotubes with Alkali-Element Modified Cu/MgO Catalyst. *Chem. Phys. Lett.* **2005**, *409*, 89–92.
31. Vander Wal, R. L.; Ticich, T. M.; Curtis, V. E. Substrate-Support Interactions in Metal-Catalyzed Carbon Nanofiber Growth. *Carbon* **2001**, *39*, 2277–2289.
32. Deng, W. Q.; Xu, X.; Goddard, W. A. A Two-Stage Mechanism of Bimetallic Catalyzed Growth of Single-Walled Carbon Nanotubes. *Nano Lett.* **2004**, *4*, 2331–2335.
33. Zhou, W. W.; Han, Z. Y.; Wang, J. Y.; Zhang, Y.; Jin, Z.; Sun, X.; Zhang, Y. W.; Yan, C. H.; Li, Y. Copper Catalyzing Growth of Single-Walled Carbon Nanotubes on Substrates. *Nano Lett.* **2006**, *6*, 2987–2990.
34. Hannon, J. B.; Kodambaka, S.; Ross, F. M.; Tromp, R. M. The Influence of the Surface Migration of Gold on the Growth of Silicon Nanowires. *Nature* **2006**, *440*, 69–71.
35. Zhou, Z.; Zhao, J. J.; Chen, Z. F.; Gao, X. P.; Lu, J. P.; Schleyer, P. v. R.; Yang, C. K. True Nanocable Assemblies with Insulating BN Nanotube Sheaths and Conducting Cu Nanowire Cores. *J. Phys. Chem. B* **2006**, *110*, 2529–2532.
36. Chen, H.; Chen, Y.; Li, C. P.; Zhang, H. Z.; Williams, J. S.; Liu, Y.; Liu, Z. W.; Ringer, S. P. Eu-Doped Boron Nitride Nanotubes as a Nanometer-Sized Visible-Light Source. *Adv. Mater.* **2007**, *19*, 1845–1848.
37. Laffont, L.; Wu, M. Y.; Chevallier, F.; Poizot, P.; Morcrette, M.; Tarascon, J. M. High Resolution EELS of Cu-V Oxides: Application to Batteries Materials. *Micron* **2006**, *37*, 459–464.
38. Drouet, C.; Laberty, C.; Fierro, J. L. G.; Alphonse, P.; Rousset, A. X-Ray Photoelectron Spectroscopic Study of Non-Stoichiometric Nickel and Nickel-Copper Spinel Manganites. *Int. J. Inorg. Mater.* **2000**, *2*, 419–426.
39. Wagner, R. S.; Ellis, W. C. Vapor−Liquid−Solid Mechanism of Single Crystal Growth. *Appl. Phys. Lett.* **1964**, *4*, 89–90.
40. Loiseau, A.; Willaime, F.; Demoncy, N.; Hug, G.; Pascard, H. Boron Nitride Nanotubes with Reduced Numbers of Layers Synthesized by Arc Discharge. *Phys. Rev. Lett.* **1996**, *76*, 4737–4740.
41. Yu, D. P.; Sun, X. S.; Lee, C. S.; Bello, I.; Lee, S. T.; Gu, H. D.; Leung, K. M.; Zhou, G. W.; Dong, Z. F.; Zhang, Z. Synthesis of Boron Nitride Nanotubes by Means of Excimer Laser Ablation at High Temperature. *Appl. Phys. Lett.* **1998**, *72*, 1966–1968.
42. Sekiguchi, T.; Koizumi, S.; Taniguchi, T. Characterization of P-N Junctions of Diamond and c-BN by Cathodoluminescence and Electron-Beam-Induced Current. *J. Phys.: Condens. Matter* **2004**, *16*, S91–S97.
43. Zhang, H. Z.; Phillips, M. R.; Fitzgerald, J. D.; Yu, J.; Chen, Y. Patterned Growth and Cathodoluminescence of Conical Boron Nitride Nanorods. *Appl. Phys. Lett.* **2006**, *88*, 093117–093119.
44. Zhi, C. Y.; Bando, Y.; Tang, C. C.; Xie, R. G.; Sekiguchi, T.; Golberg, D. Perfectly Dissolved Boron Nitride Nanotubes Due to Polymer Wrapping. *J. Am. Chem. Soc.* **2005**, *127*, 15996–15997.
45. Zhang, S. B.; Wei, S. H.; Zunger, A.; Katayama-Yoshida, H. Defect Physics of the $CuInSe_2$ Chalcopyrite Semiconductor. *Phys. Rev. B* **1998**, *57*, 9642–9656.
46. Vetter, U.; Hofsass, H.; Taniguchi, T. Visible Cathodoluminescence from Eu-implanted Single- and Polycrystal c-BN Annealed under High-Temperature, High-Pressure Conditions. *Appl. Phys. Lett.* **2004**, *84*, 4286–4288.
47. Xu, S. F.; Fan, Y.; Luo, J. S.; Zhang, L. G.; Wang, W. Q.; Yao, B.; An, L. N. Phonon Characteristics and Photoluminescence of Bamboo Structured Silicon-Doped Boron Nitride Multiwall Nanotubes. *Appl. Phys. Lett.* **2007**, *90*, 13115–13117.
48. Wu, J.; Han, W. Q.; Walukiewicz, W.; Ager, J. W.; Shan, W.; Haller, E. E.; Zettl, A. Raman Spectroscopy and Time-Resolved Photoluminescence of BN and $B_xC_yN_z$ Nanotubes. *Nano Lett.* **2004**, *4*, 647–650.
49. Kim, Y. H.; Chang, K. J.; Louie, S. G. Electronic Structure of Radially Deformed BN and BC_3 Nanotubes. *Phys. Rev. B* **2001**, *63*, 205408-1–205408-5.
50. Han, W. Q.; Yu, H. G.; Zhi, C.; Wang, J.; Liu, Z.; Sekiguchi, T.; Bando, Y. Isotope Effect on Band Gap and Radiative Transitions Properties of Boron Nitride Nanotubes. *Nano Lett.* **2008**, *8*, 491–494.

51. Kohn, W.; J., S. L. Self-Consistent Equations Including Exchange and Correlation Effects. *Phys. Rev.* **165**, *140*, A1133–A1138.
52. Perdew, J. P.; Burke, K.; Ernzerhof, M. Generalized Gradient Approximation Made Simple. *Phys. Rev. Lett.* **1997**, *78*, 1396.
53. Delley, B. Aalytic Eergy Derivatives in the Numerical Local-Density-Functional Approach. *J. Chem. Phys.* **1991**, *94*, 7245–7250.
54. Delley, B. From Molecules to Solids with the DMol(3) Approach. *J. Chem. Phys.* **2000**, *113*, 7756–7764.
55. Bergner, A.; Dolg, M.; Kuchle, W.; Stoll, H.; Preuss, H. *Ab Initio* Energy-Adjusted Pseudopotential for Elements of Groups 13−17. *Mol. Phys.* **1993**, *80*, 1431–1441.